Effect of mounting geometry on convection occurring under a photovoltaic panel and the corresponding efficiency using CFD

Michael J. Wilson and Manosh C. Paul*

Systems, Power & Energy Research Division, School of Engineering, University of Glasgow, Glasgow G12 8QQ, UK

Abstract

Computational fluid dynamics (CFD) is used to model experimental data corresponding to convection occurring under a Photovoltaic (PV) panel. Further experimental data is used to validate the model where the satisfactory agreement is received. A standardised condition is set up to allow the effect of varying three geometric parameters to be examined. These are the air gap height (10-500mm), air gap orientation angle (0-90º from the horizontal) and fluid velocity magnitude (0-3m/s). The optimum mounting conditions for the PV panel is obtained and maximised electrical efficiency found to favour angles greater than 50º and air gap heights that give an aspect ratio of 60. Mixed convection opposed to natural convection is found to be more effective, with greater efficiencies obtained for larger fluid velocities.

Key Words

Photovoltaic, Convection, Solar panel, Orientation, Cavity, Temperature, CFD

* Corresponding author: E-mail: Manosh.Paul@glasgow.ac.uk, Tel: +44 (0)141 330 8466, Fax: +44 (0)141 330 8383

Nomenclature

A	Area (m^2)
a, b, c, d, e, f	Constants
c_p	Specific heat capacity (J/kg K)
E	Energy (J)
G	Solar irradiance (W/m^2)
g	Gravitational acceleration ($9.81 m/s^2$)
h	Heat transfer coefficient (W/m^2 K)
k	Thermal conductivity (W/m K)
L	Length (m)
Nu	Nusselt number
p	Pressure (Pa)
Pr	Prandtl number
q	Heat flux (W/m^2)
Ra	Rayleigh number
Re	Reynolds number
s	Distance between plates (m)
T	Temperature (K)
u, v	Velocity components along x and y respectively (m/s)
α	Thermal diffusivity (m^2/s)
β	Expansion coefficient
γ	Efficiency correction coefficient for solar irradiance
ε	Emissivity
η	Efficiency (%)
θ	Orientation angle of panel system (°)
μ	Viscosity (kg/m s)
ρ	Density (kg/m^3)

Subscripts:

a	Ambient fluid
av	Average
f	Front of PV
p	Electrical power

pv	Photovoltaic
r	Rear of PV
rad	Radiative
s	Distance between plates (m)
sl	Solar
w	Building envelope surface

Abbreviations:

CFD	Computational fluid dynamics
DO	Discrete ordinates radiation
PV	Photovoltaic panel
STC	Standard testing conditions

1 Introduction

Although much attention has been given to studying the material properties of PV modules to enable maximum electrical efficiencies at elevated temperatures (Skoplaki et al. 2008), much less attention has been devoted to the effects of the mounting geometry of PV modules on the PV temperature and output efficiencies.

The maximum power output and electrical efficiency achievable by a PV panel is extremely dependent on the temperature of the silicon modules within the panel. Nordmann and Clavadetcher (2005) indicate that the relationship between maximum power and cell temperature is linear. Mattei et al. (2005) suggests that for crystalline silicon modules, the efficiency can drop by as much as 0.5% per 1ºC temperature increase. This may seem small, but when it is considered that currently most commercially available modules have efficiencies in the range 12-18%, and during operation, panel temperatures can rise by as much as 42ºC (Radziemska and Klugmann 2006), it becomes much more significant. Modules are tested at standard testing conditions (STC), which involve an operational temperature of 25°C, and this provides the stated electrical efficiency of a PV panel. Recent study on asymmetric compound parabolic photovoltaic concentrators by Mallick et al. (2007) also reports that the electrical conversion efficiency of the PV system is increased by about 17% when the air inlet velocity of 1.0 ms^{-1} is applied at a gap of 20 mm of the channels due to the reduction in temperature of 34.2 K of the cells compared to the cases without using any air channels.

The aim of this paper is to investigate the effect of mounting type and mounting geometry on the temperature of a PV panel (Sharp NE-80EJE). Computational Fluid Dynamics (CFD) is used to study the effects of heat transfer in the air gap between a panel and building envelope when direct mounting is used. Initial work by Brinkworth et al. (1997) introduced the importance of air-gap depth to aiding heat transfer from a PV, although only for the scenarios of vertical cladding and fixed roof angles. Therefore, here, both the air gap height and orientation angle was studied simultaneously, to develop a relationship. A CFD model has been developed and validated by using experimental data of Trinuruk (2006). Subsequent simulations have been run to study the effects on heat transfer from the panel. This allowed predictions to be made on the optimum mounting conditions for a PV panel. Considering a ‘real-life’ example, predictions of power output and efficiency could be made.

1.2 Relevant theories

A common mounting method involves 'direct mounting', where a panel is mounted on a building, offset by a small amount such that an air gap is present between the panel and the building envelope. This air gap may exist at any angular orientation between the horizontal (flat roof mounting) and vertical (wall mounting) condition. Any air gap height (distance between the panel and the building) may exist.

This air gap may be fully enclosed, open at two of the four ends, or fully open. In the first instance, the working fluid, air, is essentially trapped in the gap. In the latter cases, mass transfer occurs between the air gap and the environment. The fluid may move naturally, as a result of natural convection, or a net fluid velocity may be present, in which case mixed convection occurs. This is common in windy locations.

As the PV panel absorbs solar radiation, a number of energy transfers occur. Trinuruk (2006) analyses the heat transfer process on a PV panel and the building envelope. Consider the arbitrarily mounted PV panel shown in Fig.1. This shows an *idealised* energy balance on a PV panel; consideration is therefore not given to factors such as optical efficiency. Further investigation would be required if these were to be considered in the energy balance. By taking an energy balance approach:

$$E_{sl} = E_p + (E_f + E_r), \tag{1}$$

where the solar radiative energy (E_{sl}) is balanced with the heat energy losses at rear (E_r) and front (E_f) and the electric power (E_p). Energy can be lost from the solar side via reflected radiation, convection, and conduction. Conduction occurs to the surrounding air, and through the support frame of the PV, however, this is very small relative to convection, such that the effect can be considered to be negligible. Of the absorbed energy, some of this is converted to electrical power; the rest of the energy is lost as heat, which is transferred to the air gap. This behaviour can be represented by Eq. (2) proposed by Yang et al. (1996):

$$G = E_p + h_f \left(T_{pv} - T_a\right) + h_r \left(T_{pv} - T_{av}\right), \tag{2}$$

where G is the incident solar radiation of intensity on the panel. The final term in Eq. (2) refers only to the heat flux that flows from the PV panel into the air gap and needs to be dissipated into the air gap and either conducted through the building in the fully enclosed case, or convected into the environment in the cases of open sides. The more effectively this heat is

removed from the panel, the lower the PV temperature that can be maintained, providing the maximum efficiency. The behaviour of this thermal energy must be considered and is primarily related to the aforementioned geometric parameters.

The heat transfer from the panel is largely affected by the geometric parameters: air gap type, height of air gap, angular orientation of air gap, and fluid velocity. Only the fully enclosed and fully open air gap types are considered in this study and the remaining three will be studied more closely. The fully enclosed air gap corresponds to the experimental data used to validate the model, Trinuruk (2006). Although CFD simulation will allow the PV module temperature to be predicted, this must be related to an expected operational efficiency. Yang et al. (1996) describe the relationship between maximum power output and PV temperature to vary linearly. However, Evans (1981) proposes that the relationship between the efficiency of a PV panel at a temperature above Standard testing conditions (STC) can be described by:

$$\eta = \eta_{T_{STC}} \left[1 - \lambda_{STC} \left(T_{pv} - T_{STC}\right) + \gamma \log G\right], \tag{3}$$

where λ_{STC} and γ are the efficiency correction coefficients for temperature and solar irradiance respectively. These material properties are typically taken to be 0.0045 K^{-1} and 0.12 respectively. Often though, γ is taken as zero (Evans and Florschuetz 1978). Hence this reduces Eq. (3) to:

$$\eta = \eta_{T_{STC}} \left[1 - \lambda_{STC} \left(T_{pv} - T_{STC}\right)\right] \tag{4}$$

A better approximation for λ_{STC} can be calculated by:

$$\lambda_{STC} = \frac{1}{T_{\eta=0} - T_{STC}}. \tag{5}$$

The temperature at which the silicon PV module's efficiency drops to zero can be taken as $T_{\eta=0} = 270°C$ (Evans and Florschuetz 1978). All other parameters can be taken from the PV module manufacturer's data. This is applicable only to a specific PV panel. This value for the efficiency as calculated from Eq. (4) will be referred to as the 'adjusted efficiency'- adjusted for the particular geometric conditions only, neglecting the effect of any other variables.

3 Description of methodology

3.1 CFD modelling

Figure 2 shows the schematic of PV panel that is considered for modelling with the three important parameters such as inclination angle (θ), air gap height (s) and temperature of the PV (T_{pv}). The model of panel being considered here is Sharp NE-80EJE, an 80w, 0.6m², multi-crystalline silicon PV with stated module efficiency of 12.6%. All simulations will be based on this. When fully enclosed sides are considered, this is represented by an adiabatic (insulating) surface. The tedlar under surface of the PV, the concrete building envelope and insulation holds the properties indicted in Table 1 (Incropera and DeWitt 1996).

The governing equations of motion employed for modelling the flow and heat transfer in the air gap are written in the following forms under the Boussinesq assumption, which are the continuity (6), momentum (7-8) and energy (9) equations for a two-dimensional laminar incompressible flow.

$$\frac{\partial u}{\partial x}+\frac{\partial \mathrm{v}}{\partial y}=0, \tag{6}$$

$$u\frac{\partial u}{\partial x}+\mathrm{v}\frac{\partial u}{\partial y}=-\frac{1}{\rho}\frac{\partial p}{\partial x}+\left(\frac{\partial^2 u}{\partial x^2}+\frac{\partial^2 u}{\partial y^2}\right)+g\beta\left(T-T_a\right)\cos\theta, \tag{7}$$

$$u\frac{\partial \mathrm{v}}{\partial x}+\mathrm{v}\frac{\partial \mathrm{v}}{\partial y}=-\frac{1}{\rho}\frac{\partial p}{\partial y}+\left(\frac{\partial^2 \mathrm{v}}{\partial x^2}+\frac{\partial^2 \mathrm{v}}{\partial y^2}\right)+g\beta\left(T-T_a\right)\sin\theta, \tag{8}$$

$$u\frac{\partial T}{\partial x}+\mathrm{v}\frac{\partial T}{\partial y}=\alpha\left(\frac{\partial^2 T}{\partial x^2}+\frac{\partial^2 T}{\partial y^2}\right)-\nabla.q_{rad}, \tag{9}$$

where u and v are the velocity component along the co-ordinate systems x and y respectively. p is pressure, ρ is density, g is the gravitational acceleration, β is thermal expansion coefficient, T is temperature and α is the thermal diffusivity.

This study is interested in the effects of convection occurring under a PV panel. However, in reality this is not the only heat transfer mechanism in operation and conduction and radiation would also occur. Conduction effects are minimal and can be considered negligible. Radiation effects are more important, indeed a similar study by Moshfegh and Sandberg (1998) suggested that up to 30% of heat transferred between a heated parallel plate to another, can be attributed due to the effects of radiation. Discrete Ordinate (DO) radiation model is triggered in Fluent to allow the radiative heat transfer to occur between the PV and building surfaces

which are considered to be grey-diffusive, but the absorption and scattering coefficients for the air inside the enclosure are set to zero as it is considered to be a radiatively nonparticipating media. Moreover, in order to model the convection effectively, the Boussinesq model is used for density with the other fluid properties illustrated in Table 2 (Fluent 2007). Note that the properties of the working fluid are evaluated at the average film temperature according to $(T_{pv} + T_w)/2$, and considered to give good representation of the real conditions and are used throughout the CFD modelling and investigation.

The governing equations (6-9) are discretised by using the standard finite volume method to form a system of algebraic equations which has been solved by using an iterative process. Moreover, a 2nd order upwind discretisation scheme was set for momentum and energy with a SIMPLE algorithm to couple the velocity with pressure. A 2D, steady state, laminar, pressure based (PRESTO!) solver was used, and residuals and relaxation factors were retained as Fluent defaults (Fluent 2007). Further details can be found in the documentations of Fluent. At every iteration, mass and heat flux reports were examined to confirm convergence, and all the solutions were taken when they converged and the residuals levelled off to assigned value. The sensitivity of the numerical results with the various choices of mesh distribution used in the enclosure will be assessed and presented in the section below along with the validation of the experimental data.

3.2 Mesh refinement and validation with experiment

A 2D model of the fully enclosed air gap, as shown in Fig. 3 corresponding to the test rig set up of Trinuruk (2006), is initially modelled for the mesh refinement test. The testing rig allowed data to be taken at three points along the *x*-axis within the mid-location of the air-gap, as well as the panel temperature and building envelope temperature taken in the centre of the plate and assumed to be the average temperature. The panel was able to rotate between 0° and 90° and all readings were taken outside in 'clear sky' conditions, and it can be assumed that the ambient temperature and solar irradiation were constant.

First, the horizontal case (0°) is chosen for the mesh independence test, which is followed by the investigation of the set up of 15° (closest to location latitude) and 90° (vertical) orientations in the fully enclosed condition. The full details of the average PV and wall temperature measured at different orientations are given in Table 3 while the side walls are

considered to be adiabatic. As shown in the table, the experimental data was collected at the same time but on the different date of year. The measured top (PV) and bottom plate (wall) temperatures will be used in the model, which will allow the fluid flow, temperature profiles, the suitability of the mesh, variance of properties and the accuracy of the CFD model, to be understood. The data for the air-gap temperature will be recorded at the mid-line of the enclosure (y = 0.05m) to validate the CFD model against the experiment.

In the horizontal condition a mesh with the dimensions of 250×50 is initially generated and is deemed to be a suitable starting size for this geometry. The mesh is then refined until a trade-off between mesh accuracy and mesh size is reached; to give the most accurate results with experiment. The successive ratios are considered for the x and y directions to be 1.02 and 1.208 respectively, allowing the mesh to be finer at the edges of the enclosure, where the boundary layers are more important, hence giving a better representation of the real condition.

Fig. 4 illustrates the difference between the simulated and experimental values for each mesh dimension. The y=x line indicates ideal results, meaning the simulated temperatures are identical to those from experiment. The results obtained by the first two meshes (250×50 and 300×60) show less accuracy since they produce quite unstable results that fluctuate between the hot (PV) and cold (wall) plates. Increasing the mesh node count in each direction (e.g. 350×70, 350×75 and 400×75) gives a better accuracy compared to the experimental results. It would be explored later in Section 4 that the temperature profile inside the enclosure predicted by the higher resolution mesh shows an anticipated pattern with the ‘curls’ which are even, regular and symmetrical. The error is clearly reduced by the last three meshes, so one of these combinations could be used in the investigations. However, in terms of saving computing time, 350×70 would be chosen since this mesh confirms to be suitable for the model and gives sufficient accuracy with the experimental results.

To further confirm that this mesh and associated fluid properties are appropriate for the other two orientations, a comparison between the experimental and simulated results is shown in Fig. 5 for 15º and 90º. The agreement is quite good and acceptable. Therefore, the mesh set up of 350×70 is also sufficient for resolving the flow accurately at these two angular set ups.

4 Preliminary assessment of convection under the experimental conditions

The effects of convection taking place in the air-gap on the efficiency of the PV panel will be analysed for the three angular orientations according to the experimental boundary conditions mentioned in Table 3. Fig. 6(a), which is at 0° (horizontal case), shows that the thermal boundary layers are thick and conduction is the main heat transfer mechanism. If the effects of radiation were being ignored, it would be most likely that the temperature profile would have isotherms along the length in the *x*-direction. However, the effect of radiation produces 'curls' of convection as the fluid absorbs the radiation emitted by the heated upper panel, corresponding to the theory of the beginning of a small convection cell, but it cannot develop further due to the retarding viscous forces of the surrounding fluid. The pocket of fluid absorbing the radiation does not gain enough energy this way to enable it rise into the thick 'hot' layer above it, and can only rise very slightly. The Rayleigh ($Ra = \frac{\rho g \beta \Delta T L^3}{\mu \alpha}$) number is calculated as 236, 731 although this has no relationship to the Nusselt number ($Nu = \frac{hs}{k}$) that is taken as 1 regardless for this horizontal, heated upper plate situation. Moreover, in Table 4 the efficiency drops by 2.4% from STC, which if exposed to maximum solar irradiation would be a reduction in power output of approximately 2W. This may seem small, but for an array, this would be more significant.

In Fig .6(b), when the angle of PV is 15°, it can be seen that the thermal boundary layers have started to develop along the length, with maximum thickness occurring at the apex and base for the hot and cooler surfaces respectively. Natural convection has started to occur, and a convection cell is developing. The flow for this condition would be slow as the buoyancy forces are just managing to overcome the retarding viscous forces and expected to increase for larger rotations. The core of the fluid (green area) is most likely to be stagnant due to the combination of low angle of orientation and slow convection cell velocity. To confirm this further, the magnitude of the fluid velocity is taken along a line perpendicular to the PV, mid way and along the length of the height of the enclosure and presented in Fig. 7. A convection cell is evident, as the two plates exhibit opposite and equal fluid velocity and at the midpoint between the plates the fluid is almost stationary. Greater velocities will enhance heat transfer from the PV module, reducing temperature, and maximising PV efficiency. The Rayleigh number is also calculated and found to be 1129686 and the associated average heat transfer coefficient, *h*, to be 8.09 W/m² K.

Furthermore, this angle (15°) corresponds approximately to that of the Latitude of the test location (13.73°N) and assumed that it would receive the maximum incident solar irradiation on the surface. This corresponds to a greater temperature, and hence the greater change in efficiency of -4% (Table 4). Had experimental data about the power output have been available, it would have been interesting to investigate angling the PV directly into the sun. This may have had a negative effect on the power output due to the increased panel operating temperature, or perhaps this would be overcome by the increase in the solar irradiation allowing greater power output.

In the vertical case (90°), Fig. 6(c) shows that a full convection cell has developed and the thermal boundary layers have thinned. The Rayleigh number in this case is found to be 574116, with the associated average heat transfer coefficient, *h*, to be 4.98 W/m² K. The velocity profile in Fig. 7, with respect to a line horizontally through the mid-height of the enclosure, shows that the magnitude is almost double compared to the 15° case and there is a much larger stagnant fluid area in the middle. The drop in efficiency from STC is predicted to 3.2% as shown in Table 4. Despite the smaller drop in efficiency, it can be assumed that this would not generate as much electrical energy compared to the 15° situation, as there is a greater deviance from the angle of optimum incident solar radiation.

4.1 Simulation conditions for further investigations

The convection occurring under a PV panel will now be further investigated. Considering that the model is now validated against the experimental results, a standardised situation is created that would allow only the effect of the geometric parameters to be studied. The following conditions applied:

- A constant heat flux is present along the length of the PV, equalling that dissipated into the gap under normal operation - 260W/m.
- The building envelope is set as an adiabatic boundary to give a ‘worst case’ scenario.
- Open sides are considered.
- Angles of orientation of 15º, 30º, 45º and 90º from the horizontal are studied.
- Bulk fluid velocities of 0, 1, 2 and 3 m/s are studied. Note a wind velocity of zero gives the case of natural convection.
- Air gap heights of 0.01m, 0.02m, 0.03m, 0.04m, 0.05m, 0.1m, 0.15m, 0.2m and 0.25m are studied, giving corresponding aspect ratios from 4.8 to 120.

- Ambient air at atmospheric pressure and 25ºC.
- The surface materials of the PV and building are still considered to be tedlar and concrete, respectively.

Natural and mixed convection are considered individually and results are presented in Sections 5 and 6 respectively. Preliminary solutions are run to assess basic correlation between the parameters above. Simplifying assumptions will be made where possible and complete investigation is executed along with data reduction to obtain relationships.

5. Results of natural convection

Preliminary simulations are run first to allow the assessment of the basic correlation between natural convection and the orientation angle and aspect ratio. Average PV panel temperatures are determined and will be discussed with respect to the variables. An angle of 15° is taken as constant for a variable air gap height, and a constant air gap height of 100mm taken for variable orientation angle.

From Fig. 8, it can be seen that with increasing orientation angle, the temperature of the PV panel decreases, and this can be associated with greater heat transfer from the surface to the fluid. After approximately 50° the temperature begins to level and successive rotation does not greatly increase heat transfer. At small angles, larger gains can be made, and as a direct consequence the angles 15°, 30° and 45° will be chosen for closer examination later, in addition to 90° to allow an effective control. These results are obtained at a channel height, *s*, of 100mm with an aspect ratio of 12 (L/s), so it is unlikely that the flow would have left the hydrodynamic entrance region and become fully developed at this dimension.

The effect of the angle on the average PV temperature in Fig. 8 is further investigated by the effective opening size which is defined as the distance between the ends of the plates in the *x*-direction as

$$x_{eff} = s\sin\theta. \qquad (10)$$

Larger angles give greater effective opening sizes. Since motion in the vertical direction is attributed to the effect of buoyancy, increasing the (perpendicular) effective opening size at the top of the enclosure increases buoyancy flow between the control volume and ambient

environment, and hence increases heat transfer from the PV. This is the principle behind a solar chimney.

Figure 9 illustrates the decrease in PV temperature is rapid and linear for small separations until about 0.02m. But between 0.02 and 0.04m, the decrease slows. The temperature then rises at 0.05m before falling steadily with increasing the air gap size. The rapid decrease up to 0.02m is indicative of the transition of heat transfer from conduction to convection and is caused by the fluid which remains largely static and the frictional forces retard motion. As the air gap size is increased, the convection takes over, and the larger opening allows a fluid motion to develop. At this point, a buoyancy induced fluid motion exists, and boundary layers form on either plate. To understand the fact more clearly, a simulation on infinitely separated plates is run, and a maximum boundary layer thickness of 22mm is measured, so it can be concluded that fully developed flow would first occur between 0.02 and 0.04m separation. Furthermore, the small rise in temperature at 0.05m is caused probably due to the boundary layers having just enough space to fully develop but still run close enough together that they interfere. The boundary layers beyond 0.05m are examined and found to be independent, and has impact on the steady temperature drop with increasing separation. Onur and Aktas (1998) reports similar findings at *s*=0.024m and 0.06m which relate to the discovered trends at s=0.02m and 0.05m respectively.

5.1 Data reduction and further investigation on natural convection

The simulations are repeated for the angles of 15°, 30°, 45°, and 90° from the horizontal and the air gap height is varied. For each simulation, the average PV temperature is taken and dimensionless relations are formed. For natural convection, the Nusselt number is usually a function of the Rayleigh and Prandtl numbers:

$$Nu = f\left(Ra, \mathrm{Pr}\right). \tag{11}$$

However, the Prandtl number does not vary largely over the temperature ranges associated with the data and can be taken as constant. This gives the Nusselt number as a function of the Rayleigh number only, the relating function defined by the geometric parameters θ, s and L such that

$$Nu_s = f\left(Ra_s, \frac{s}{L}, \theta\right). \tag{12}$$

For each orientation angle, the mathematical form of the dimensionless relationship is expected to be (Khedari et al. 2002)

$$Nu_s = a\left[\left(\frac{s}{L}\right)Ra_s\right]^b, \qquad (13)$$

where *a* and *b* are constants derived for each orientation angle from the line of best fit and compared to the literature where available. In Table 5, we find that for angles of 45 and 90 degrees, the results from simulation sufficiently agree with those in the literature, Bashaya et al. (1999) and Onur and Aktas (1998). Should the variable sinθ be introduced, a single correlation can be formed that relates all the variables:

$$Nu_s = c\left[\left(\frac{s}{L}\right)Ra_s\sin\theta\right]^d, \qquad (14)$$

where *c* and *d* are constants, and again from the line of best fit, as shown in Fig. 10, it can be concluded that for the case of natural convection, the relationship between the variables can be described by the following equation

$$Nu_s = 0.5203\left(\frac{s}{L}Ra_s\sin\theta\right)^{0.2981}. \qquad (15)$$

However, no values of the constants are found in literature which would allow this result to be compared to other work.

To establish the impact of the air gap height on the temperature of the PV panel at a specified orientation, it is desirable that the effect is quantified, using Eq. (4). This plot of the adjusted efficiency is shown in Fig. 11, which gives a direct numerical value of efficiency for this specific PV panel, at each mounting type and geometry. This result confirms that large angles and small aspect ratios are associated with greater adjusted efficiency directly resulting from the greater heat transfer and lower PV temperature (Figs. 8 and 9).

6. Results of mixed convection

Again, preliminary simulations are run to attain basic correlation with bulk fluid entrance velocities of 1, 2 and 3m/s. An angle of 15º is also taken as constant for variable air gap height, and a constant air gap height of 100mm taken for variable orientation angle.

From Fig. 12, it can be seen that for fluid at a velocity, the average temperature of the PV remains almost constant irrespective of angle of orientation. In fact, larger velocities are less

affected by the change in orientation angle. The angular effect on the PV temperature is therefore assumed to be negligible and overall increasing the fluid velocity decreases the average PV temperature.

The effect of the air gap height can be seen in Fig. 13; all curves exhibit the same momentary decrease in temperature at a gap size of 0.02m, and this is expected to be due to a velocity boundary layer effect. To assess this, the velocity profiles are recorded at the exit of the channel and shown in Fig. 14. At a plate spacing of 0.02m, and at all velocities, the velocity profiles (top frame) indicates that a fully developed flow occurs at the exit channel and the boundary layers are unidentifiable within the profiles. A further increase in the air gap size results in the flow not developing fully as clearly shown by the blunt exit velocity profiles in Fig. 14 (bottom frame) and the heat transfer from the panel decreasing. This causes the temperature to rise for the subsequent air gap height of 0.03m. This can be further attributed by the fact that the breakdown of conduction occurring when the velocity profile no longer exhibits fully developed flow, and the boundary layers become fully independent. Moreover, the thermal boundary layers also do not combine and a developing temperature profile exists. When the geometry tends towards infinitely separated plates from 0.03m onwards, the average PV temperature falls steadily, accordingly.

6.1 Data reduction and further investigation on mixed convection

A relationship between the Nusselt and Reynolds numbers is also established for mixed convection taking the Prandtl number as constant and the mathematical form of this dimensionless relationship is expected as

$$Nu_s = e\left[\left(\frac{s}{L}\right)\mathrm{Re}_s\right]^f, \qquad (16)$$

where e and f are constants derived from the simulation data. The velocity term features in the Reynolds number, but the orientation angle is not featured as is regarded as negligible. Data according to Eq. (16) is plotted in Fig. 15, and the line of best fit the relationship between the variables for mixed convection can be described by the following equation

$$Nu_s = 1.0822\left[\left(\frac{s}{L}\right)\mathrm{Re}_s\right]^{0.4623}. \qquad (17)$$

To provide a quantitative evaluation of the effect of the gap size, Eq. (4) is used again to find the adjusted efficiency of the PV panel and plotted in Fig. 16 for the three different wind velocities. This expresses a direct numerical efficiency for the different mounting geometry. This figure confirms that the aspect ratios in the range 43-120 are associated with greater adjusted efficiency directly resulting from lower PV temperature. Moreover, the adjusted efficiency rises with the rise in wind velocity because of the lowering temperature of PV with the higher wind flow on the PV. Overall, a maximum value of about 12% efficiency is obtained at an aspect ratio of 60 and wind velocity of 3m/s.

7 Conclusion

A CFD model was created to investigate the effects on convection occurring under a PV panel. The model was validated using experimental data collected from Trinuruk (2006). Three geometric parameters (the air gap height, the orientation angle and the presence and magnitude of a bulk fluid velocity) were considered and the effect of these on the average PV panel temperature was investigated.

Generally, panel temperature was minimised, maximising the electrical efficiency when the following conditions were satisfied:

- Natural convection: Orientation angles above 50º from the horizontal, and larger air gap heights,
- Mixed convection: Air gap heights that lead to an aspect ratio of 60, and large fluid velocities. The angular effect can be considered negligible.

In addition, simulation constants were found to develop dimensionless relationships to relate all variables. These were as follows:

- Natural convection: $$Nu_s = 0.5203\left(\frac{s}{L}Ra_s \sin\theta\right)^{0.2981}$$
- Mixed convection: $$Nu_s = 1.0822\left[\left(\frac{s}{L}\right)\mathrm{Re}_s\right]^{0.4623}$$

The simulation results were also used to give ‘adjusted efficiencies’ which indicated numerical values for each geometric condition. These considered a panel with a stated STC efficiency of 12.6%. For natural convection the best efficiencies of 10.75-10.92% were attained for an angular orientation of 90˚. For mixed convection, the best efficiencies of 11.27-11.98% were achieved for a fluid velocity of 3m/s.

Two-dimensional simulations were performed. In reality, the depth is finite and cross-flow will occur, which will result in mixing of the different temperature fluids in the third dimension. Further work on this project would involve creating a 3D model and investigate the effects of mounting geometry parameters on the performance of the PV panel. Furthermore, a uniform heat flux, which is comparable to heat flux on a standard panel and not the solar irradiation, is applied along the length of the PV panel for both the natural and

mixed convection setups. Additional factors such as panel type, and internal and external optical effects caused by the solar irradiation are ignored as it is the resulting heat that is relevant to the study of convection and the effects it has behind the panel. In a future work the issue of optical effect where the solar irradiation (Mallick et al. 2007) is required to be used as an input to the panel could also be further investigated.

Acknowledgement

The authors like to thank Miss P. Trinuruk (who was an IAESTE Fellow at the Department of Mechanical Engineering, University of Glasgow) and her colleagues in King Mongkut's University of Technology, Thailand for sharing their experimental data with us. The authors also thank the anonymous reviewers for their valuable comments and suggestions on the earlier version of this paper, which have served to improve the manuscript.

References

Baskaya, S., Aktas, M.K. & Onur, N., (1999) Numerical simulation of the effects of plate separation and inclination on heat transfer in buoyancy driven open channels. *Heat and Mass Transfer*, 35, pp. 273-280.

Brinkworth, B.J., Cross, B.M., Marshall R.H. & Yang, H., (1997) Thermal regulation of photovoltaic cladding. *Solar Energy*, 61(3), pp. 169-178.

Evans, D. L. & Florschuetz, L. W., (1978) Terrestrial concentrating photovoltaic power system studies. *Solar Energy*, 20(1), pp. 37-43.

Evans, D. L., (1981) Simplified method for predicting photovoltaic array output. *Solar Energy*, 27(6), pp. 555-560.

FLUENT 6.3 (2007) Tutorials Guide. USA: Fluent INC.

Incropera, F.P. & DeWitt, D.P., (1996) *Introduction to Heat Transfer*, 3rd Ed., United States, John Wiley and Sons Inc.

Khedari, J., Yimsamerjit, P. & Hirunlabh, J., (2002) Experimental investigation of free convection in roof solar collector. *Building and Environment*, 37, pp. 455-459.

Markvart, T., (1994) *Solar Electricity*, Chichester, England, John Wiley and Sons Ltd.

Mallick T. K., Eames, P. C. & Norton, B., (2007) Using air flow to alleviate temperature elevation in solar cells within asymmetric compound parabolic concentrators. *Solar Energy*, 81, pp. 173–184.

Mattei, M., Notton, G., Cristofari, C., Muselli, M. & Poggi, P., (2005) Calculation of the polycrystalline PV Module temperature using a simple method of energy balance. *Renewable Energy*, 31, pp. 553-567.

Moshfegh, B. & Sandberg, M., (1998) Flow and heat transfer in the air gap behind photovoltaic panels. *Renewable and Sustainable Energy Reviews*, 2, pp. 287-301.

Nordmann, T. & Clavadetscher, L., Accessed online on 23/02/2010, *Understanding temperature effects on photovoltaic system performance*, http://www.iea-pvps.org/products/download/pap2_033.pdf

Onur, N. & Aktas, M.K., (1998) An experimental study on the effect of opposing wall on natural convection along an inclined hot plate facing downward. *Int. Comm. Heat and Mass Transfer*, 25 (3), pp. 389-397.

Radziemska, E. & Klugmann, E., (2006) Photovoltaic maximum power point with illumination and temperature. *Journal of Solar Energy Engineering*, 128, pp. 34-39.

Skoplaki, E., Boudouvis, A.G., & Palyvos, J.A., (2008) A simple correlation for the operating temperature of photovoltaic modules of arbitrary mounting. *Solar Energy Materials & Solar Cells*, 92, pp. 1393-1402.

Trinuruk, P., (2006) Electricity generation and heat gain on photovoltaic roofs in Thailand. *MPhil Thesis, King* Mongkut's University of Technology, Thonburi, Bangkok, Thailand.

Yang, H.X., Marshall, R.H. & Brinkworth, B.J., (1996) Validated simulation for thermal regulation or photovoltaic wall structures. *PVSC*, 25, pp. 1453-1456.

Material	*Density, ρ (kg/m³)*	*Specific heat, c_p (J/kg K)*	*Thermal conductivity, k (W/m K)*	*Radiation Emissivity, ε*
Tedlar	1475	1130	0.14	0.893
Concrete	1444	1229	0.5868	0.6
Insulation	32	835	0.038	1

Table 1: Material Properties (Incropera and DeWitt 1996)

Parameter	*Model*	*Value*
Density, ρ (kg/m³)	Boussinesq	1.1806
Specific heat, c_p (J/kg K)	Constant	1005
Viscosity, μ (kg/m s)	Constant	1.858e-5
Thermal conductivity, k (W/m K)	Constant	0.02568
Thermal expansion, β (1/K)	Constant	3.47e-3

Table 2: Properties of air

Angular position	*Time and Date*	*Temperature of PV, T_{pv} (K)*	*Temperature of wall, T_w (K)*
0º	9am, 10/01/2007	303.72	297.54
15º	9am, 08/11/2006	308.02	301.01
90º	9am, 12/02/2007	306.32	301.1

Table 3: Experimental data: Measured temperature of the PV and wall (Trinuruk 2006)

Angular position	*Rayleigh number (Ra)*	*Heat Flux (W/m)*	*STC Efficiency (%)*	*Adjusted Efficiency (%)*	*Change in Efficiency (%)*
0º	236,731	27.3	12.6	12.3	- 2.4
15º	1,129,686	35.8	12.6	12.1	- 4.0
90º	574,116	29.1	12.6	12.2	- 3.2

Table 4: Effects of convection on efficiency at different angular positions

Orientation	*Simulation*		*Literature*	
	a	*b*	*a*	*b*
15°	0.333	0.3065	-	-
30°	0.413	0.3007	-	-
45°	0.4659	0.2965	0.498 [m]	0.258 [m]
90°	0.5728	0.2831	0.577 [n]	0.243 [n]

[m] Bashaya et al. (1999) [n] Onur and Aktas (1998)

Table 5: Constants from simulation and from literature

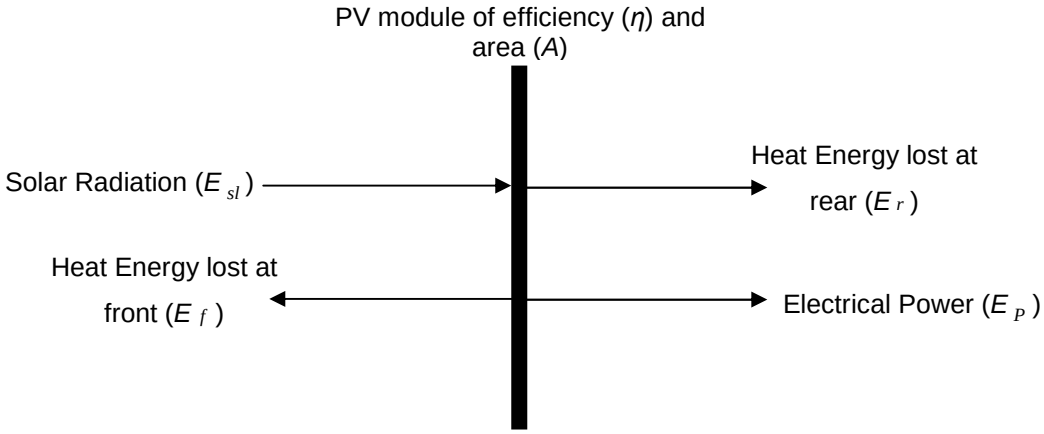

Figure 1: Energy balance on an arbitrarily mounted PV panel

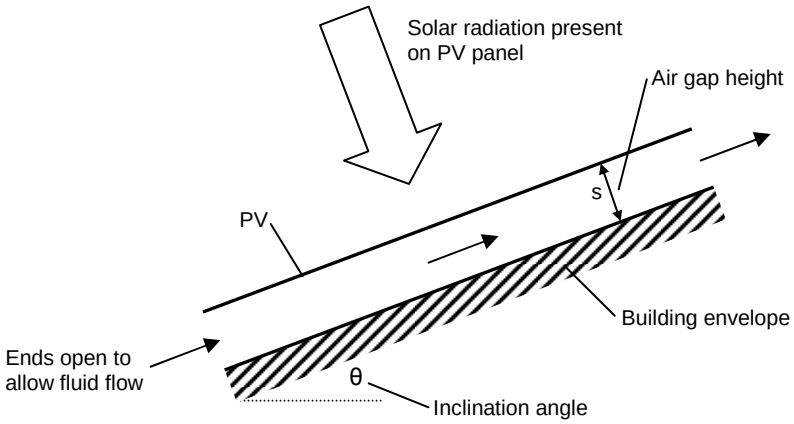

Figure 2: Schematic description of mode-open sides shown

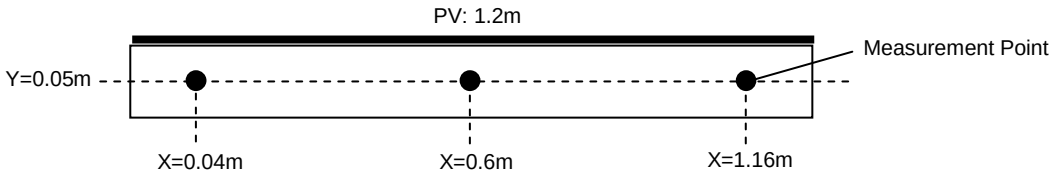

Figure 3: Temperature measurement locations

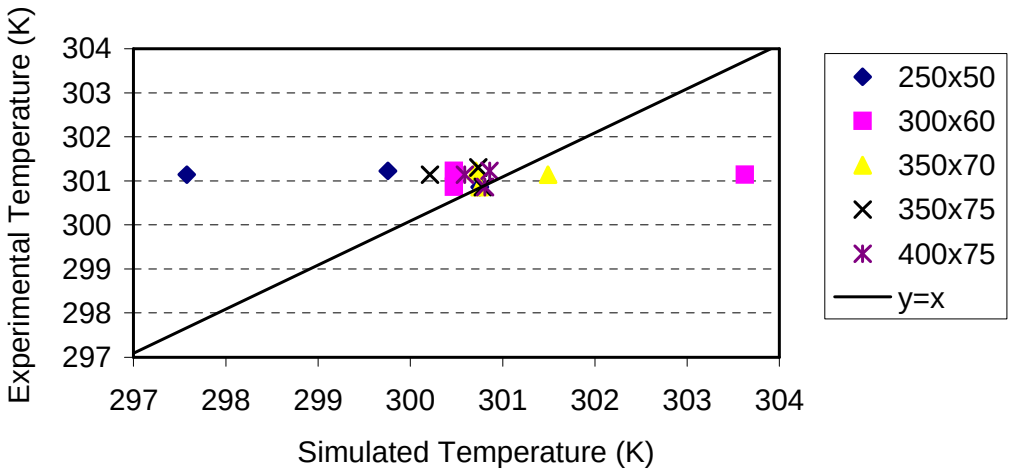

Figure 4: Comparison of experimental and simulated data for different mesh sizes at 0º (horizontal). Ideal results lie on line indicated by y=x.

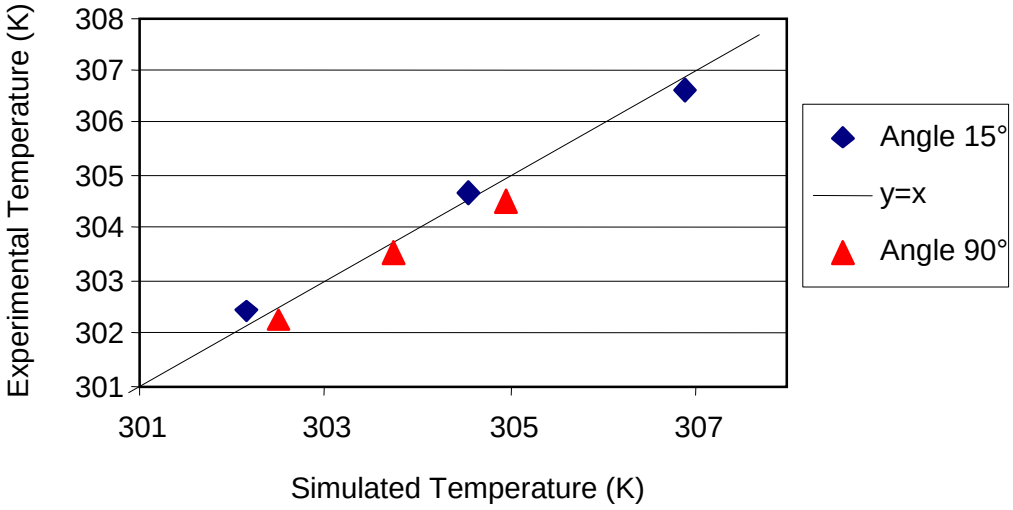

Figure 5: Comparison of experimental and simulated data at 15º and 90º (vertical). Ideal results lie on line indicated by y=x.

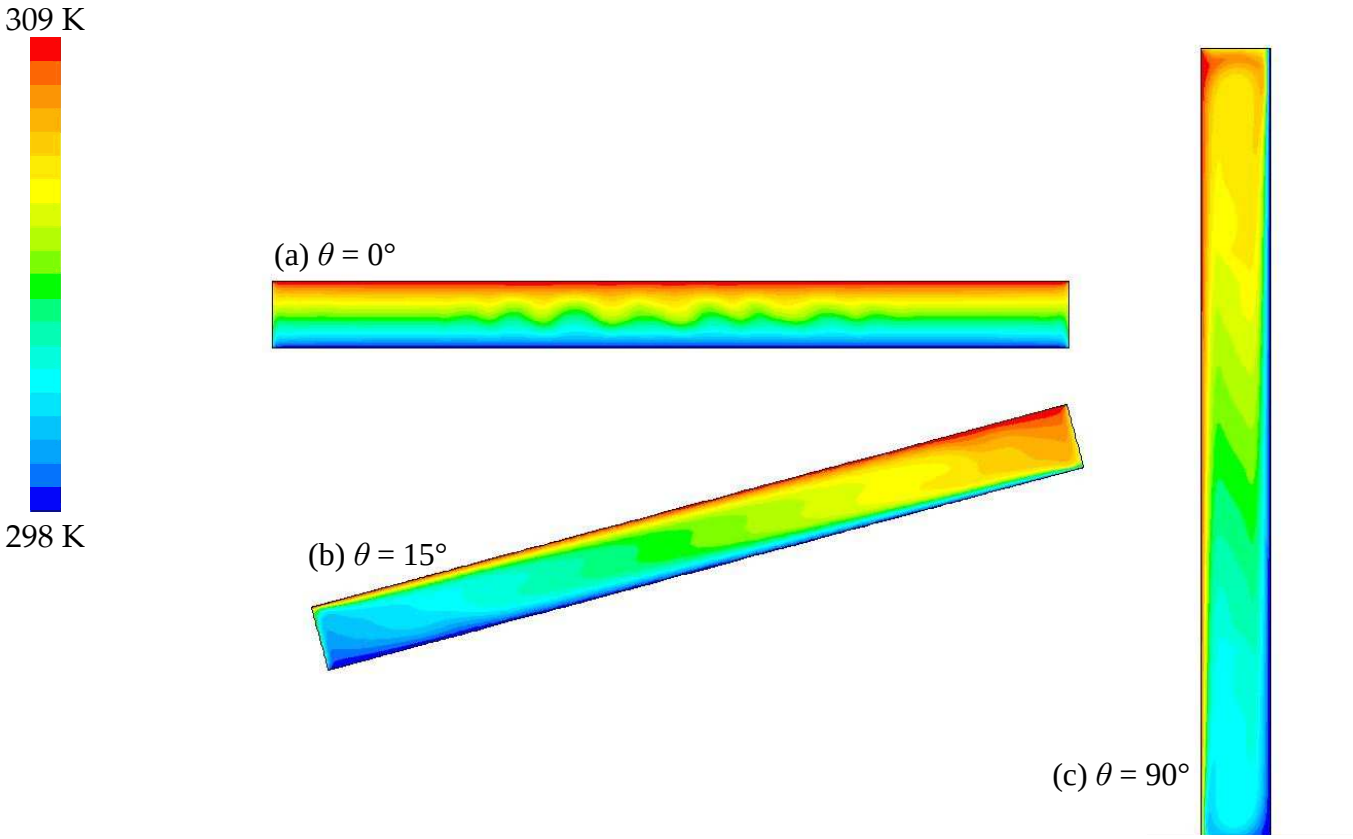

Figure 6: Temperature profile inside the enclosure at different angular positions, indicating the highest (309K) and lowest (298K) temperatures

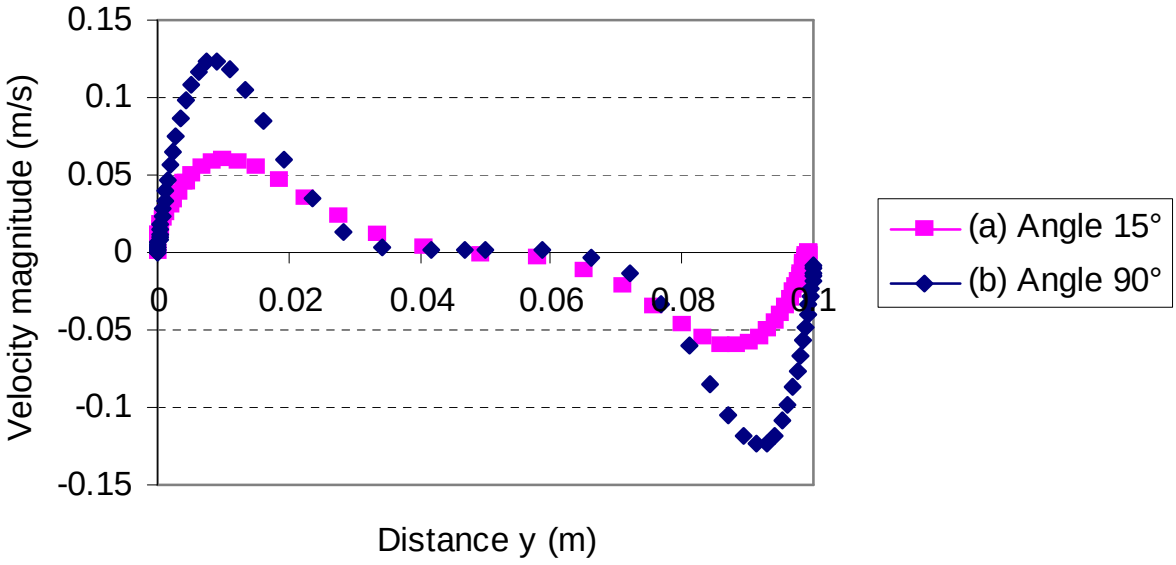

Figure 7: Fluid velocity magnitude along the mid line of the enclosure at different orientations

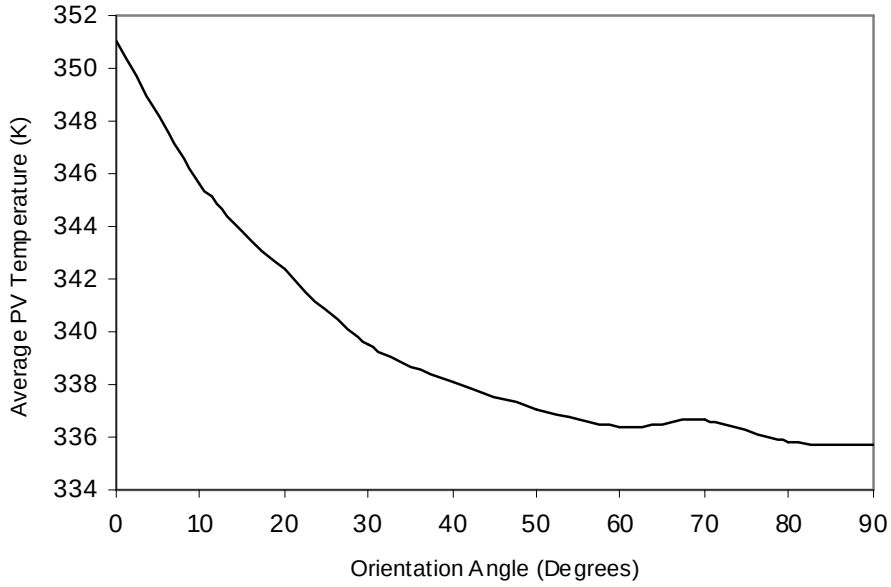

Figure 8: Average PV temperature with respect to angle of orientation when *s* =100mm, with an ambient air temperature of 298K

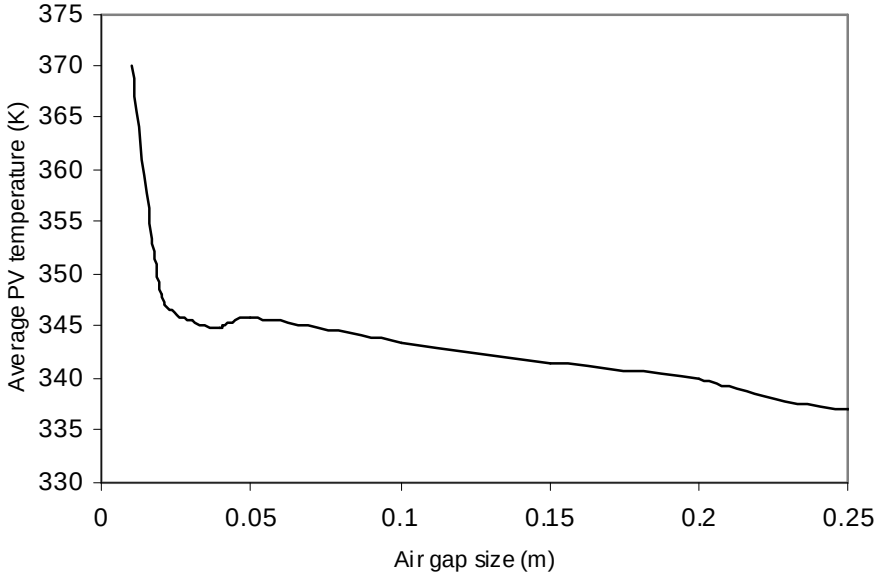

Figure 9: Average PV temperature with respect to air gap size when θ =15°, with an ambient air temperature of 298K

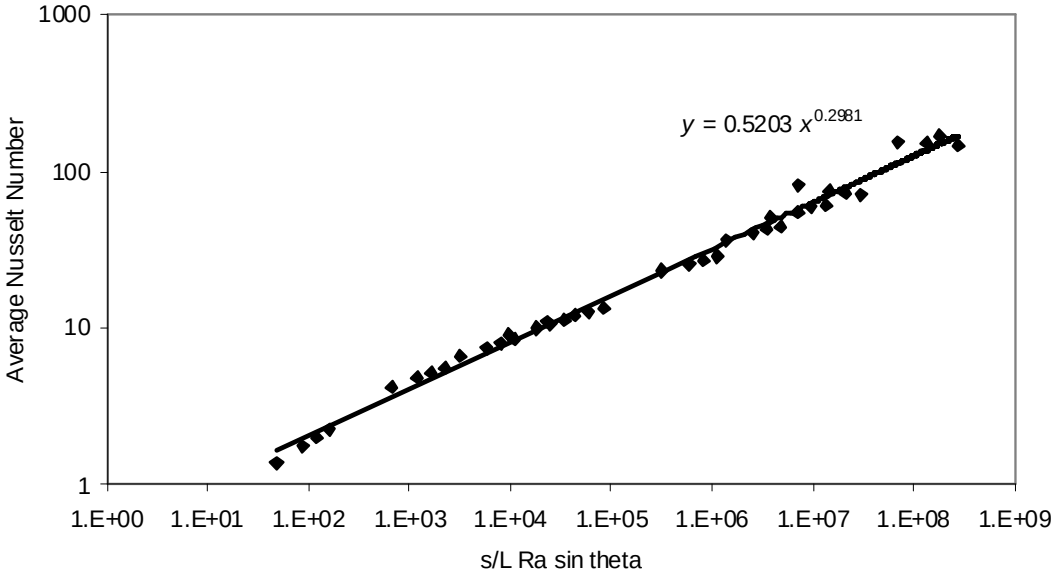

Figure 10: Dimensionless relationship between Rayleigh and Nusselt numbers

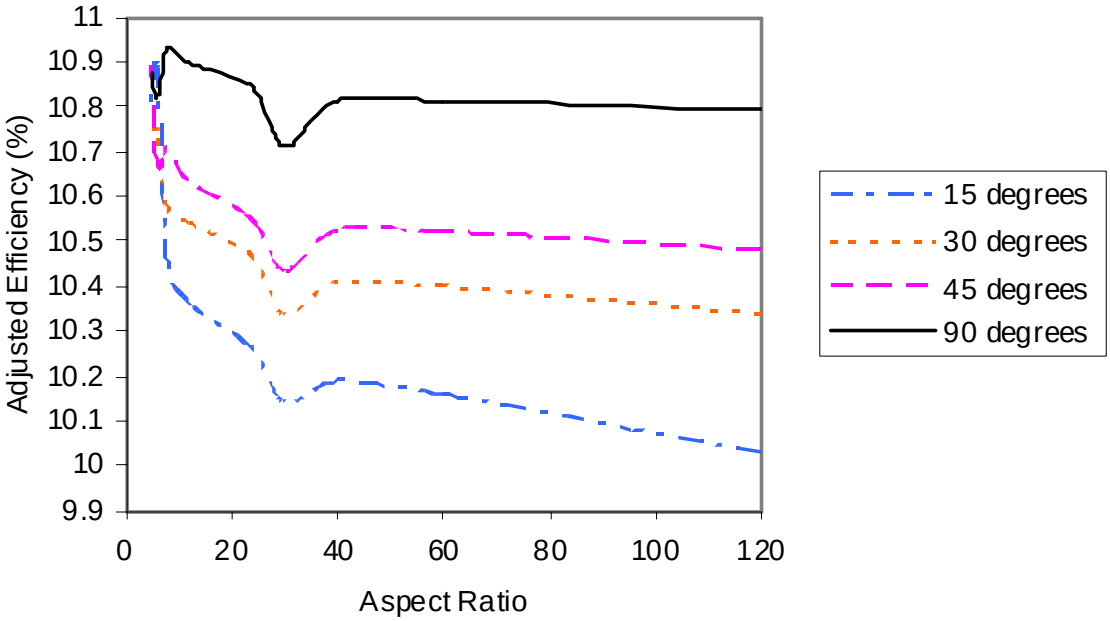

Figure 11: PV efficiency at different mounting angles and aspect ratios

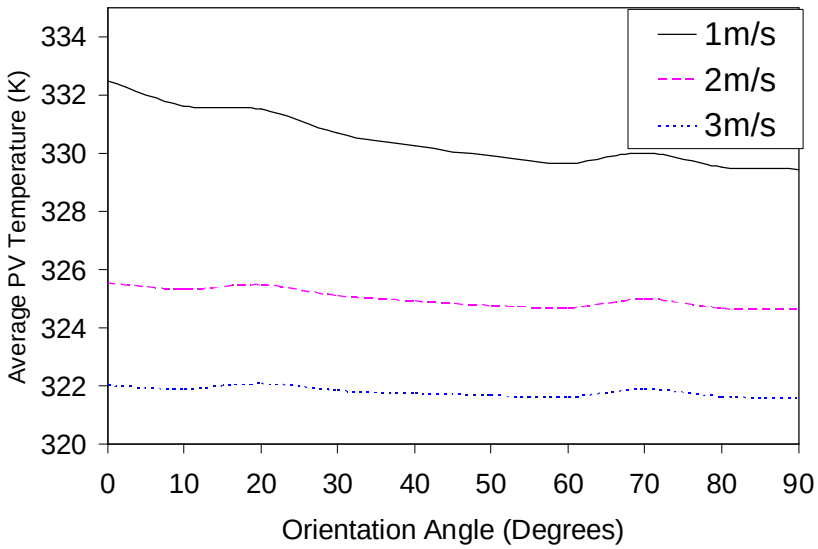

Figure 12: Average PV temperature with respect to angle of orientation when *s* =100mm

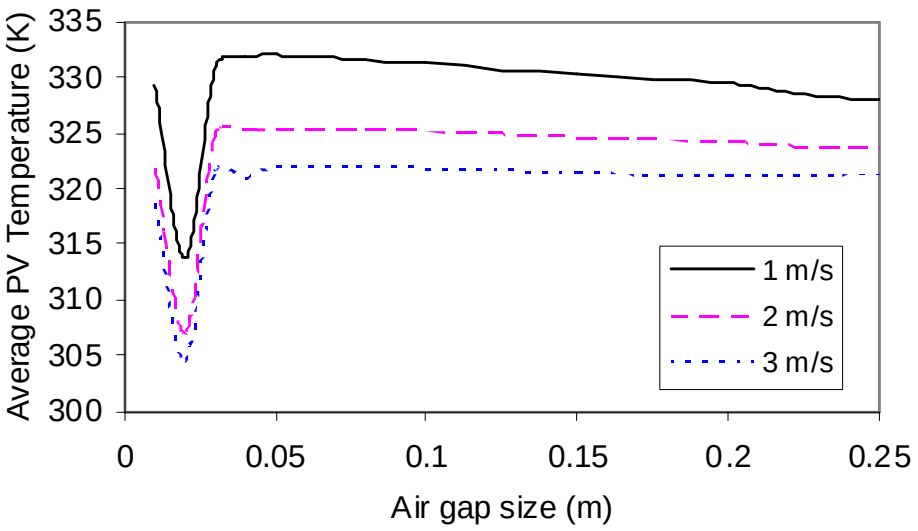

Figure 13: Average PV temperature with respect to air gap size at θ =15°

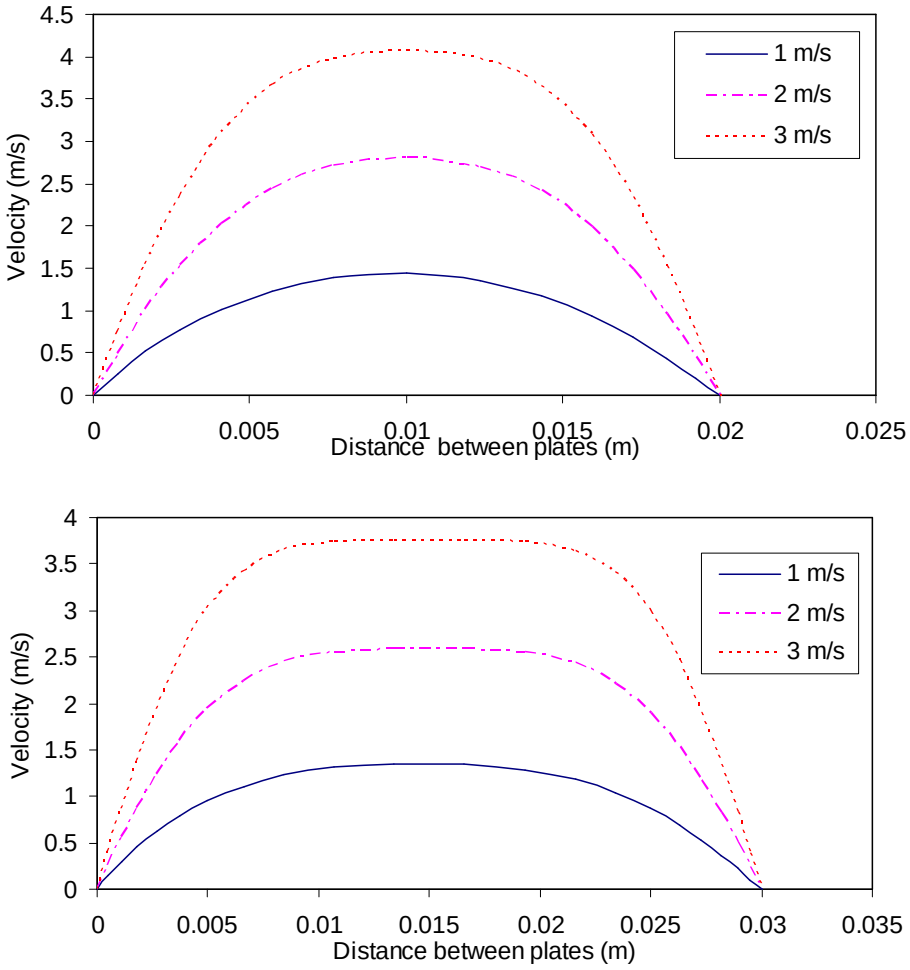

Figure 14: Exit velocity profiles for 0.02m (top) and 0.03m air-gap

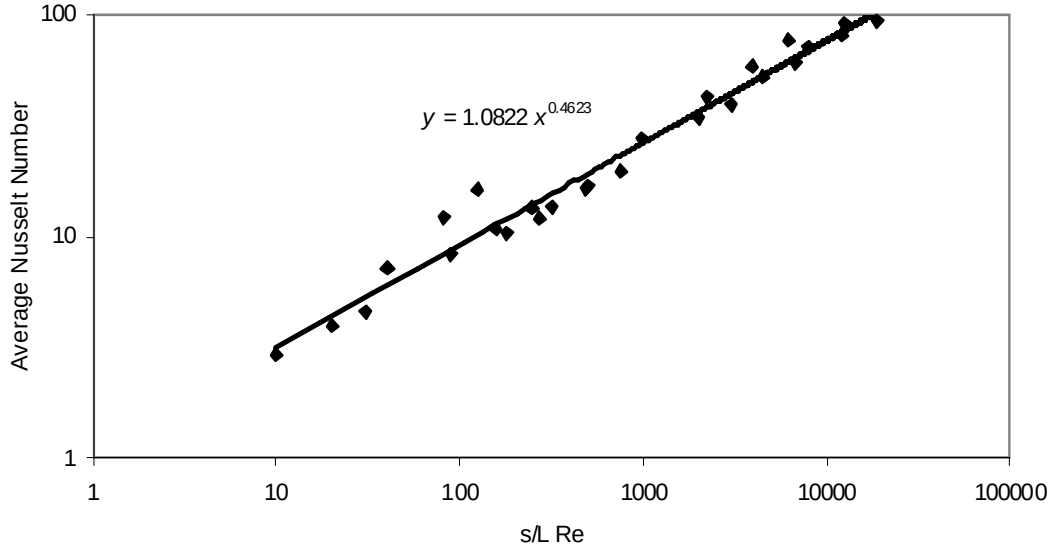

Figure 15: Dimensionless relationship between Reynolds and Nusselt numbers

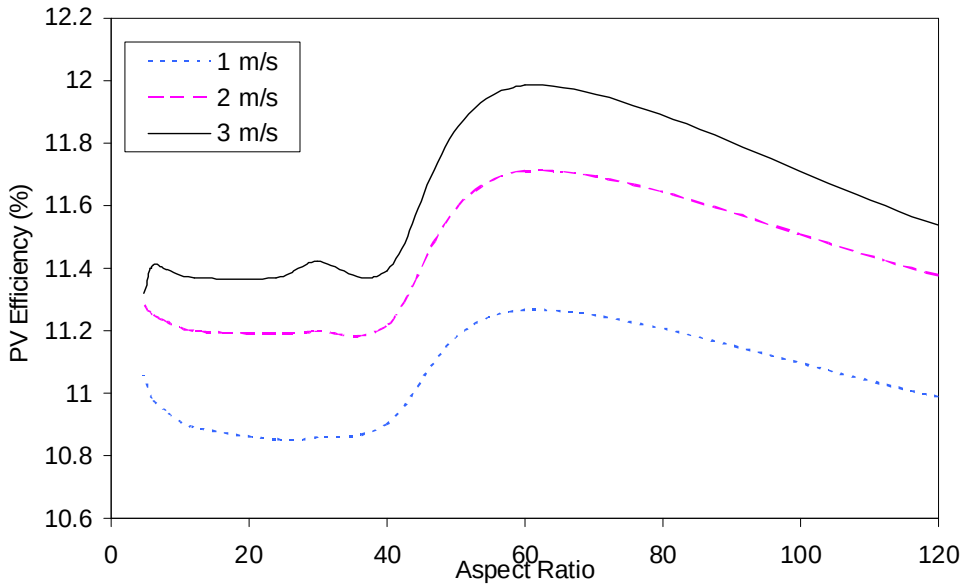

Figure 16: PV adjusted efficiency at different fluid velocities and aspect ratios